Supplementary Material

1. Theoretical Analysis

1.1 Particle separation by numerical prediction

To predict the separation performance of this method, the distribution of $\nabla|\boldsymbol{E}|^2$ around the orifice and the motion of particles were numerically simulated. For the simulations, the following assumptions were made:

(1) The thermo-physical properties of the liquid are constant and have no thermal effect on the flow field and particle velocity;

(2) The particle and the walls of the channel are non-porous, and do not react with the surrounding liquid;

(3) The rotation of the particle does not affect the particle's translation motion;

(4) The solution is diluted enough to neglect the electrostatic interaction between the particles;

(5) Polarization is weak at the interface of the two-phase solution and is not sufficient to affect the distribution of the electric field in the channel.

1.1.1Mathematical models

In this study, ionic liquid is filled into the S-channel and the rest channels are filled with another electrolyte solution(Figure 1). An electric potential is applied between the wells C and E. Particles are released from x_0 which is the center of section A and move towards section D in the main channel. The particles are pushed away from the orifice by the DEP force and the vertical distance from the orifice is defined as separation distance.

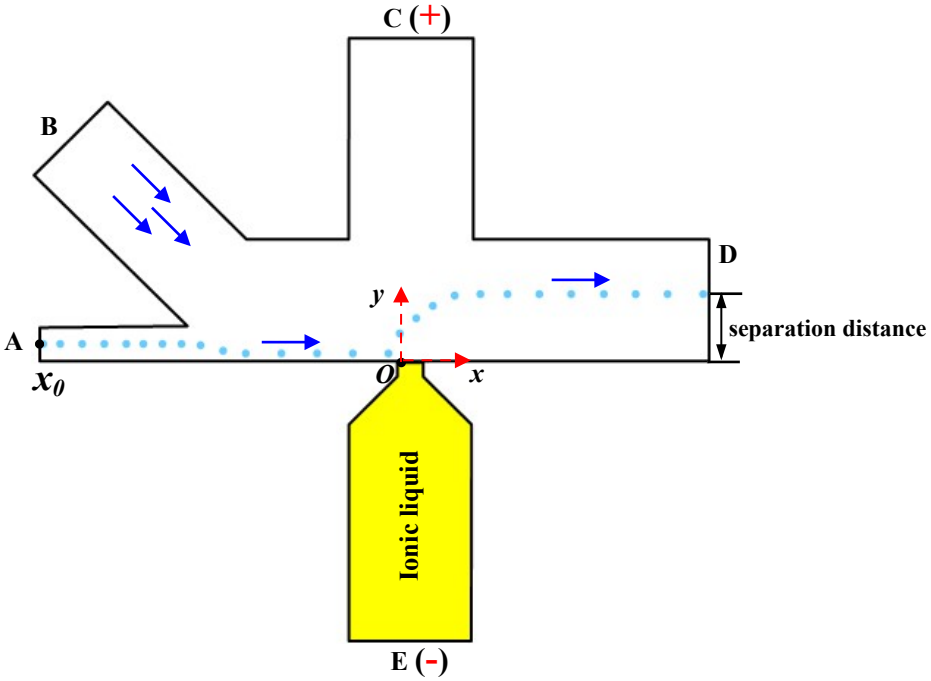

Figure 1 Schematic diagram of particle separation

1) Electric field

The electric potential(V) in the channel is governed by Laplace's equation:

$$\nabla^2 V = 0 \tag{1}$$

and the local applied electric field strength(E) in the channel is given by

$$\boldsymbol{E} = -\nabla V \tag{2}$$

The applied gradient of the electric field squared ($\nabla|\boldsymbol{E}|^2$) in the channel is given by

$$\nabla|\boldsymbol{E}|^2 = \sqrt{\left(\frac{\partial \boldsymbol{E}^2}{\partial \mathrm{x}}\right)^2 + \left(\frac{\partial \boldsymbol{E}^2}{\partial \mathrm{y}}\right)^2 + \left(\frac{\partial \boldsymbol{E}^2}{\partial \mathrm{z}}\right)^2} \tag{3}$$

The boundary condition for the electric field is

$$\boldsymbol{n} \cdot \boldsymbol{E} = 0 \tag{4a}$$

where $\boldsymbol{n}$ is the unit normal vector pointing from the boundary surface,
the boundary condition of end C is

$$V = V_{\mathrm{a}} \tag{4b}$$

the boundary condition of the end E is

$$V = 0 \tag{4c}$$

2) Flow field

The flow field in the channels is governed by the Navier-Stokes equation (Eq. 5) and the continuity equation (Eq. 6):

$$\rho \boldsymbol{U} \cdot \nabla \boldsymbol{U} = -\nabla p + \mu \nabla^2 \boldsymbol{U} + \boldsymbol{F} \tag{5}$$

$$\nabla \cdot \boldsymbol{U} = 0 \tag{6}$$

where ρ is the density of the liquid, μ is the viscosity of the liquid, $\boldsymbol{U}$ is the velocity vector, ∇p is the pressure gradient, $\boldsymbol{F}$ is the body force. In this study, the flow velocity of the fluid in the microchannel is low and its Reynolds number is small. Therefore, in Eq.6, the inertia term ($\rho \boldsymbol{U} \cdot \nabla \boldsymbol{U}$), which is much smaller than the viscous term ($\mu \nabla^2 \boldsymbol{U}$), can be neglected. For the body force $\boldsymbol{F}$, Because the buffer solution is electric neutrality and the net charge density is non-zero only in the double layer (EDL)， the body force $\boldsymbol{F}$ is zero except in the EDL. In addition, the thickness of the EDL is very small (nanometer) which is negligible in comparison with the size of the microchannel. Therefore, there is no need to solve the flow field in the thin EDL. Instead, we use a slip velocity boundary for the flow field in the microchannel.

the boundary conditions of end A is

$$\boldsymbol{p} = \boldsymbol{p}_{\mathrm{a}} \tag{7a}$$

the boundary conditions of the end C is

$$\boldsymbol{p} = \boldsymbol{p}_{\mathrm{c}} \tag{7b}$$

the boundary conditions of the end D is

$$\boldsymbol{V} = 0 \tag{7c}$$

The ionic liquid remains stationary in the separation channel during the experiment, the boundary conditions of the end E, end C and the PBS-ionic liquid interface

$$\boldsymbol{U} = 0 \tag{7d}$$

the boundary conditions of the end D is

$$\boldsymbol{p} = 0 \tag{7e}$$

The wall of the channel is subject to the electroosmotic slip boundary condition

$$\boldsymbol{u} = \frac{\varepsilon_0 \varepsilon \zeta}{\mu} \boldsymbol{E} \tag{7f}$$

Where ε_0 is the dielectric constant of the vacuum, ε is the dielectric constant of the fluid, and ζ is the zeta potential at the fluid-PDMS interface.

3) Particle Motion

The instantaneous particle position x_{p} can be determined by integrating the particle velocity and the initial position(x_0):

$$x_{\mathrm{p}}(t) = x_0 + \int_0^t \boldsymbol{u}_{\mathrm{p}}(\tau) d\tau \tag{8}$$

where x_0 represents the initial position of a particle and t is the time from the initiation. In a fixed frame of reference, the translational motion of a particle is governed by Newton's second law

$$m_{\mathrm{p}} \frac{d\boldsymbol{u}_{\mathrm{p}}}{dt} = \boldsymbol{F}_{\mathrm{ext}} \tag{9}$$

where m_p represents the mass of the particle and $\boldsymbol{F}_{\mathbf{ext}}$ is the resultant of the external force of the particle.

To simplify particle motion simulation, the Lagrangian tracking method is used to predict

particle motion. This correctness of this method on particle motion prediction has been well proved. For this method, only the effect of the solution flow and the electrical field on a moving particle is considered. The effects of the particle on the flow and electrical fields are neglected. The forces exerted on the particle are the drag force by the fluid flow ($\boldsymbol{F}_{\mathbf{D}}$), the DEP force ($\boldsymbol{F}_{\mathbf{DEP}}$) and the electrophoresis force field ($\boldsymbol{F}_{\mathbf{EP}}$):

$$\boldsymbol{F}_{\text{ext}} = \boldsymbol{F}_{\text{D}} + \boldsymbol{F}_{\text{DEP}} + \boldsymbol{F}_{\text{EP}} \tag{10}$$

For a creeping flow, the drag force on aspherical particles is given by Stoke's law

$$\boldsymbol{F}_{\text{D}} = 6\pi\mu\text{R}(\boldsymbol{u} - \boldsymbol{v}) \tag{11}$$

Where μ is the dynamic viscosity of the fluid, R is the particle radius, u is the velocity of fluid flow, and v is the velocity of the particle.

The DEP force exerted on a spherical particle is given by

$$\boldsymbol{F}_{\text{DEP}} = -2\pi\varepsilon_{\text{m}} r^3 \left(\nabla \left|\boldsymbol{E}\right|^2\right) \tag{12}$$

The EP force exerted on a spherical particle is expressed as

$$\boldsymbol{F}_{\text{EP}} = Q\boldsymbol{E} \tag{13}$$

where Q is the total surface charges of the particle and the expression is

$$Q = 4\pi\varepsilon_{\text{m}}\varepsilon_0 R(1+\kappa R)\zeta_{\text{p}} \tag{14}$$

Where ε_{p} and R are the dielectric constant and the radius of the particle, respectively. κ is the Debye–Hückel parameter and $\boldsymbol{\zeta_p}$ is the zeta potential on the surface of the particles. For the symmetric electrolytes in the water phase, κ is given by

$$\kappa = \sqrt{\frac{2n_\infty z^2 e^2}{\varepsilon_{\text{p}}\varepsilon_{\text{m}} k_B T}} \tag{15}$$

where $n_\infty(\text{m}^{-3}) = N_A C_0$ is the bulk ionic number concentration with $N_A = 6.022\times10^{23}$/mol the Avogadro constant and C_0 (1 mol/m^3 =10^{-3}M) the ionic concentration of the ions in the water; z = 1 is the valence of the ions, e=1.602× 10^{-19}C is the elementary charge, k_B = 1.38×10^{-23}J/K is the Boltzmann constant, and T =298 K is the absolute temperature.

In this study, for simplicity, the initial velocity of the particle is set as:

$$\boldsymbol{v}_0 = 0 \tag{16}$$

The initial position x_0 is set at the center of end A.

Table 1 shows the relevant parameters used in the simulations.

Table 1 Parameters used for the simulations

Viscosity of PBS	μ=1.01 mPa·s
The permittivity of vacuum	ε_0=8.85×10^{-12} F/m
The density of polystyrene particles	ρ_p=1050 kg/m^3
The permittivity of polystyrene particles	ε_p=2.55
The permittivity of PBS	ε=80
zeta potential of PBS-PDMS interface	ζ=-57 mV
zeta potential of particle in PBS solution	ζ_p=-25 mV

2 Numerical simulation

Figure 2 shows the geometric model of the channel. The origin of the Cartesian coordinates is set at the left corner of the orifice (Figure 1). To reduce the amount of calculation time, the length of the channels was all shortened to 1/6 of their original length. Other size parameters, such as the width and depth of the channels are not changed.

The 3D numerical model described above is solved by COMSOL MULTIPHYSICS in this study. To improve the accuracy of the calculation, finer meshes are used for the narrow orifice and separation areas of the main channel. Furthermore, mesh independence was examined by calculating the values of the $\nabla|\boldsymbol{E}_a|^2$ under different numbers of elements. It was found that when the total number of elements is between 2758435 and 3409574, the value difference is less than 0.5%. Therefore, the total mesh number used in the simulation was not less than 2758435.

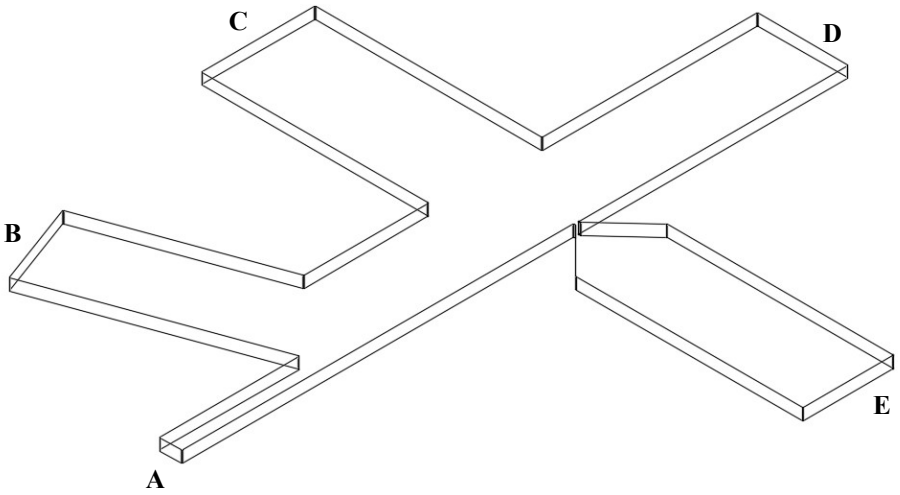

Figure 2 Geometric model of the channel

2.1 Simulation and comparison of the electric field in a shortened channel

In order to reduce the amount of calculation time, the length of the channels was all shortened to 1/6 of their original length. Therefore, the applied voltage should be carefully determined in the simulation to make the electric field distribution the same as that in the experiments (votage=100V). The following section will simulate and compare the electric field.

There are two cases of the size parameters of the channel. One is that all the size parameters of the channel are consistent with the channel used in the experiment. In this case, in order to simulate the electric field in the channel during the experiment, the boundary condition of C is set as potential V_a is 100V. In the other case, the length of the channel is reduced to 1/6 of the experimental channel, and the width and length parameters are consistent with the channel used in the experiment. The potential of C is used as a boundary condition and set to a different value in order to compare the simulation result with the previous case. Other boundary conditions and governing equations about the electric field are consistent with the simulation part of the main text.

To improve the accuracy of the calculation, finer meshes are used for the narrow orifice and separation areas of the main channel. Furthermore, mesh independence was examined by calculating the values of the $\boldsymbol{E}$ under different numbers of elements. It was found that when the total number of elements is between 3127951 and 34728601, the value difference is less than 0.5%. Therefore, the total mesh number used in the simulation was not less than 3127951.

Figure 3 shows the simulation results of electric field strength at the orifice. The black line is the simulation result of the electric field strength at the interface under experimental conditions (external power supply is 100V), and the red line is the simulation result of the 18.5 V power supply after the length of all the channels is shortened to be 1/6 of the original ones. It is clear that the simulation results of electric field strength at the interface are consistent in the above two cases. Therefore, to avoid the influence of the shortened channel on the electric field intensity in the channel, the boundary condition of C was set as 18.5V in particle trajectory simulation under experimental conditions.

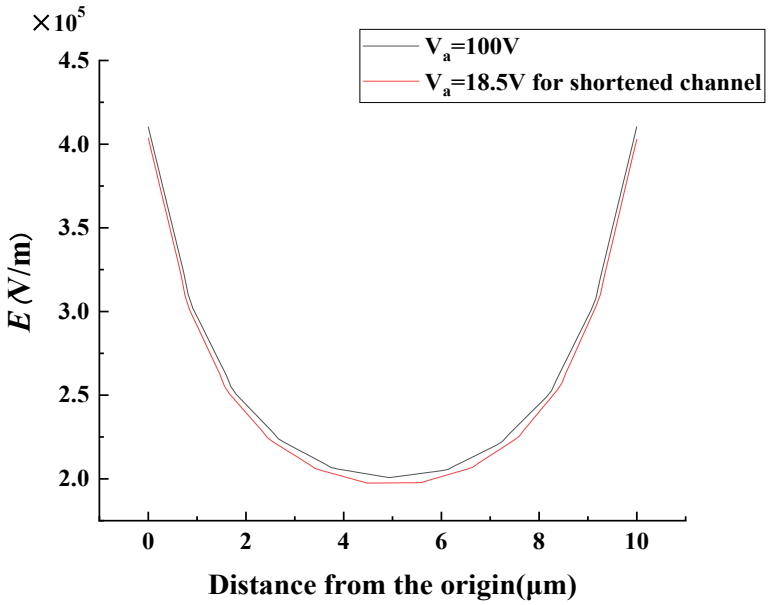

Figure 3 The electric field strength at the interface

2.2 Pressure boundary conditions for the simulation of particle trajectories

In the experiment, 1μm and 2μm particles pass through a higher magnification objective lens at a slower speed to obtain a clearer trajectory. Therefore, the boundary conditions of 1μm and 2μm in the flow field are different from those of 2μm and 4μm.

For the case of 1 μm and 2 μm, the boundary conditions of end A is

$$\boldsymbol{P}_a=29 \text{ Pa} \tag{17a}$$

the boundary conditions of the end C is

$$\boldsymbol{P}_c=40 \text{ Pa} \tag{17b}$$

For the case of 2 μm and 4 μm, the boundary conditions of end A is

$$\boldsymbol{P}_a=30 \text{ Pa} \tag{18a}$$

the boundary conditions of the end C is

$$\boldsymbol{P}_c=42 \text{ Pa} \tag{18b}$$

Other boundary conditions and governing equations about the flow field are consistent with the main text in two cases.